STUDYING REPLICATION ORGANELLES USING ADVANCED FLUORESCENCE MICROSCOPY
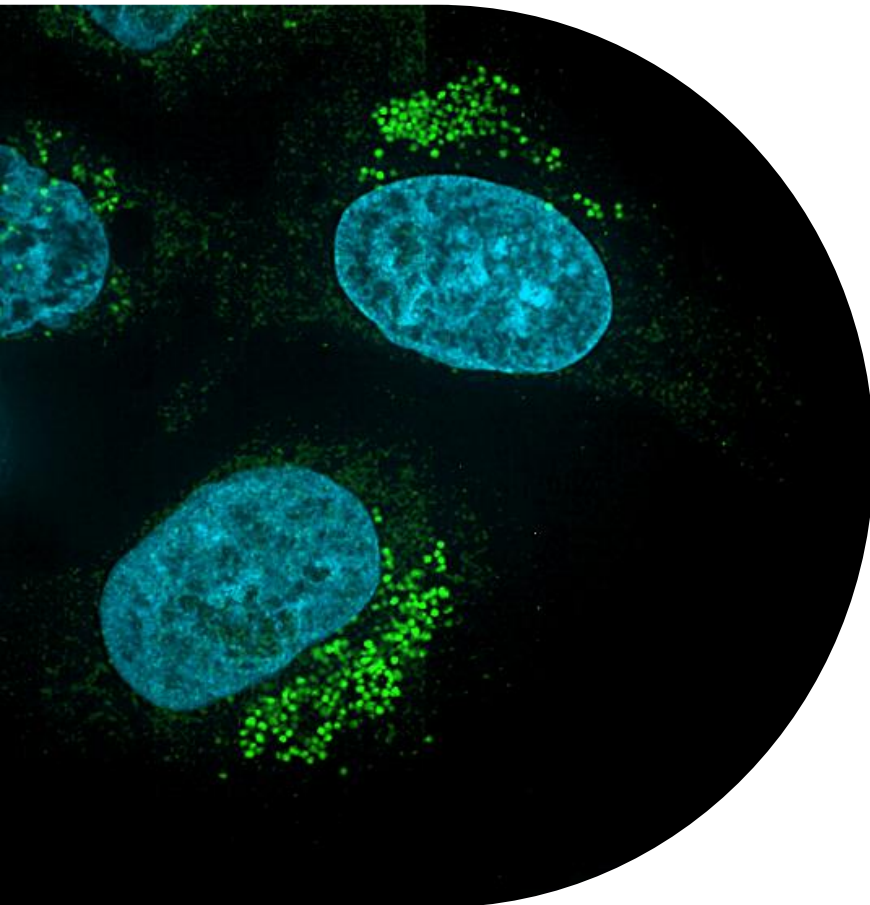
Master thesis

UTRECHT UNIVERSITY

Anna-Sophie Schlemmer

Daily supervisor

Dr. Heyrhyoung Lyoo

Examiners

Prof. Dr. Frank van Kuppeveld
Ass.-Prof. Dr. Richard Wubbolts

Table of contents

Abstract

The enterovirus genus comprises many human pathogens such as poliovirus, coxsackievirus and rhinovirus. For efficient replication, enteroviruses induce membrane rearrangements which require the interaction between viral and host factors such as PI4KB, ACBD3 and 3A. Although interactions between these proteins have been intensively studied, their localization at replication organelle (RO) membranes is unknown. To investigate components of ROs in-depth, we established protocols to study coxsackievirus B3 (CVB3) ROs using expansion microscopy (ExM) and super-resolution microscopy (SRM), i.e. Olympus SoRaSpin10 system. Our data is the first evidence of 2A localization. The use of SRM allowed us to visualize the localization of the viral protease 2A at different time points of infection in greater detail. In addition, we could locate 3A at an early time point after infection (i.e. 3 h p.i.), which was hardly attainable with conventional immunofluorescence microscopy. Our data suggest that imaging at earlier time points might be possible. Moreover, both viral proteins were visualized as dotted structures which have not yet been observed. We demonstrate the potential for in-depth visualization of these viral proteins and their colocalization with host factors using super-resolution microscopy. The Olympus SoRaSpin10 system offers the possibility to combine SRM with live-cell imaging. Thus, tracking viral protein localization, RO formation and its dynamics could be further investigated.

Layman's summary

Viruses ensure their survival by infecting cells, where they replicate to generate new virus particles that can infect other cells. Viruses have developed different strategies to replicate efficiently inside a cell. One of these strategies is the formation of unique structures, so-called replication organelles (ROs). Numerous human enteroviruses such as polioviruses, rhinoviruses and coxsackieviruses, form ROs, making ROs an ideal target for designing an antiviral drug. Therefore, it is essential to understand the formation and composition of ROs in detail.

We studied ROs using super-resolution microscopy (SRM) and expansion microscopy (ExM). Both methods are based on confocal microscopy. The principle of confocal microscopy is the absorption of light at a certain wavelength by a specific molecule, a fluorophore. The fluorophore is located at the site that we want to study, e.g. by binding to a protein that is found at ROs. After absorption, the fluorophore emits light again that can be detected and localized. SRM requires an advanced microscope that can process the images after acquisition to obtain higher resolution. Unlike SMR, ExM relies on additional sample (i.e. infected cells) preparation before imaging. Normally for imaging, cells are grown on coverslips (i.e. glass slides). For ExM, cells are transferred from the coverslip onto a gel. The gel is expanded, as expected from the name, which leads to the expansion of the entire sample. Therefore, no advanced microscope is needed to obtain higher resolution.

To study viral infection, cells are infected and fixed at a certain time point, for example, 5 h post infection. The viral proteins, 2A and 3A, that we want to study were labeled with a fluorophore. We were able to visualize 2A for the first time and showed its localization at numerous time points post infection. We located 3A at 3 h post infection which has not been possible with conventional confocal microscopes. Our work shows the potential to study ROs using super-resolution microscopy, thereby contributing to developing an antiviral drug against enteroviruses.

Introduction

Enteroviruses are non-enveloped viruses with a positive-sense, single-stranded RNA (+RNA) genome and belong to the family of *Picornaviridae*. This genus includes many clinically and economically important human pathogens such as polioviruses (PV), coxsackieviruses (CV) and rhinoviruses (RV) that cause a variety of diseases, like encephalitis and myocarditis (1). For most of these pathogens, no treatment is available yet.

All + RNA viruses share a replication strategy which involves the formation of unique viral replication organelles (ROs). The interaction between viral and host proteins can lead to rearrangements of intracellular membranes into new membranous structures that provide a platform for viral genome replication (2–4). Enteroviral ROs were shown to be dynamic structures that change their morphology during infection. Early in infection, most ROs have been visualized as single membrane tubules (SMTs). These SMTs can transform into double-membrane vesicles or multilamellar structures as infection precedes (5,6).

One of the proteins that has a crucial function in RO formation or expansion, is the viral protein 3A. Respectively, its interaction with different host factors and its role in the recruitment of proteins and lipids to RO membranes have been extensively studied (7,8). 3A induces disassembly of the Golgi apparatus and can inhibit ER-to-Golgi transport (9,10). Another role of 3A lies in the accumulation of specific lipids in RO membranes (Fig. 1). 3A binds to the acyl-CoA binding domain containing protein 3 (ACBD3), a Golgi-resident protein, promoting the recruitment of phosphatidylinositol-4-kinase-III-β (PI4KB) to RO membranes (11–13). PI4KB leads to a phosphatidylinositol-4-phosphate (PI4P) rich environment that attracts viral polymerase 3D^{pol} and cellular factors, such as oxysterol-binding protein (OSBP) (14–16). OSBP imports cholesterol into ROs and in exchange, PI4P is hydrolyzed by a phosphatase in the ER (17,18). As a result, RO membranes have a unique composition of lipids which is high in PI4P and cholesterol (19).

Another viral protein that was shown to promote cellular lipid accumulation, is the viral protease 2A. 2A is the first protein of the second polyprotein (P2) of CVB3, which can free the P2-P3 domain from P1. The protease needs to cleave itself at its C-terminus before it can interact with any host factor. 2A is mainly known to counteract the host's innate immune responses (20,21). Moreover, 2A is required for the activation of fatty acid import and it can

interact with the sterol regulatory element binding protein 1 (SREBP1), the major transcriptional factor in lipogenic gene expression (22,23). 2A was shown to mediate phosphatidylcholine (PC) synthesis by inducing translocation of CCTα (see below). Generally, the localization of this protein during viral proliferation is unclear and little is known about its interaction with cellular organelles. Hence, it has to be further investigated whether 2A is associated with ROs or contributes to their formation.
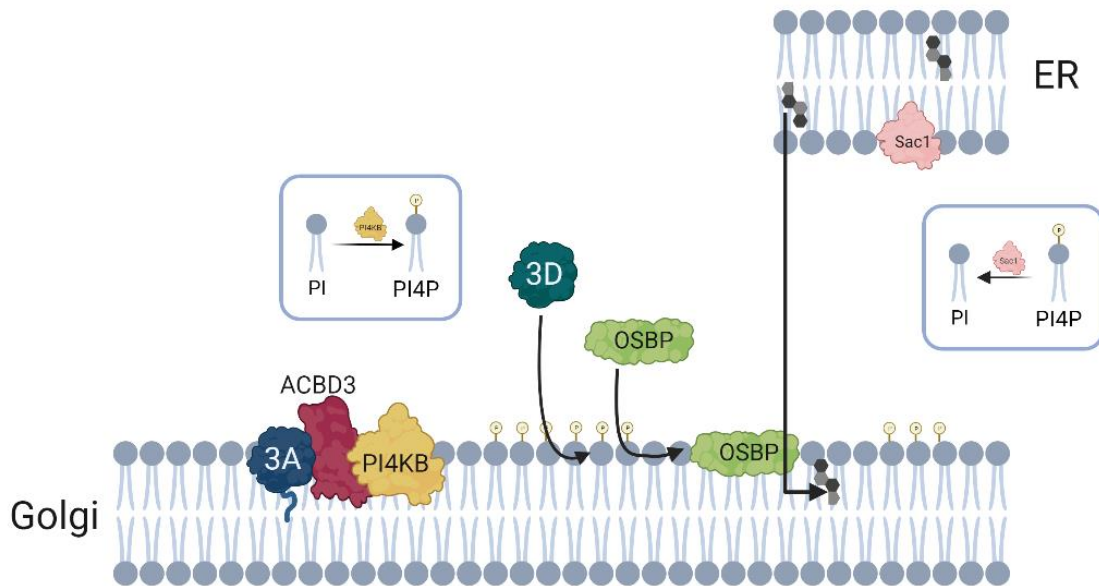

Figure 1: Schematic presentation of PI4P accumulation induced by 3A at RO membrane. 3A interaction with PI4KB is mediated by ACBD3. PI4KB converts PI to PI4P creating a PI4P-rich environment at the RO membrane. 3D and OSBP are attracted to the membrane. OSBP imports cholesterol against the energy gradient and PI4P is released from the RO membrane to the ER where it is hydrolyzed back to PI. Created with Biorender.com.

There is growing evidence that other lipids such as PC are involved in RO formation. During viral infection, phospholipids are synthesized from neutral lipids that are stored in lipid droplets (LDs) (7,19). In the case of PC, CTP-phosphocholine-cytidyl transferase alpha (CCTα), the key enzyme of PC synthesis, is translocated from the nucleus to the cytoplasm where it can interact with the membranes of ROs. The proteolytic activity of 2A is required for this translocation (24). It has been confirmed that PC synthesis inhibits the formation of ROs, though the proteins that are involved in the association between ROs and CCTα remain to be further investigated. Furthermore, LDs form molecular contact sites (MCSs) with ROs indicating a relevant role of LDs in membrane rearrangements induced by viruses (25).

Enteroviral ROs have been extensively studied using electron microscopy (EM) and conventional confocal microscopy. EM has demonstrated the dynamic nature of ROs and revealed MCSs between cellular organelles, in specific the Golgi apparatus, ER, LDs, and ROs

(6,25). Despite its high resolving power, EM is not only laborious and time-consuming but also cannot target proteins specifically. Even though EM can be combined with light microscopy to identify regions of interest, the resolution remains too low to pinpoint the specific localization of a protein. With confocal microscopy, the localization of a target protein can be better visualized. However conventional microscopes will not suffice to visualize molecular networks like the microtubule network or protein distribution with higher spatial accuracy. Consequently, numerous super-resolution microscopy (SRM) techniques have been established to obtain even more details of the cellular environment.

Expansion microscopy (ExM) is a volumetric fluorescence nanoscopy technique that can be performed using conventional microscopes. ExM is defined by the physical expansion of the sample in an isotropic fashion. Practically, ExM consists of 5 steps, fixation and protein labeling, anchoring, polymerization, homogenization and expansion (Fig. 2). The volume is enlarged about 100 times which leads to an effective resolution of approximately 75 nm compared to conventional microscopy where the resolution limit is 300 nm (26,27). To date, protocols have been published that allow enlargement of the biological specimen up to 1000 times (28).
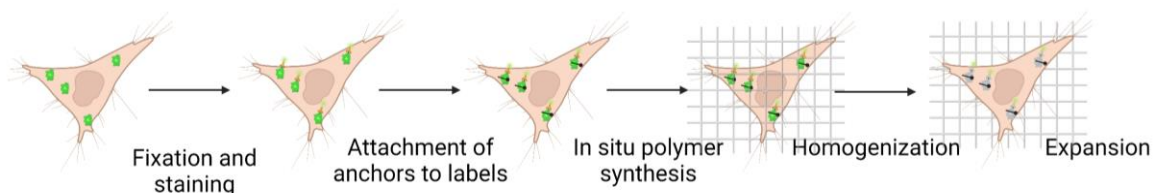

Fixation and staining — Attachment of anchors to labels — In situ polymer synthesis — Homogenization — Expansion

Figure 2: Graphical illustration of the ExM protocol. First, cells are fixed and the protein of interest is labeled with a fluorescent dye. Secondly, a chemical (Acryloyl-X) is added that interacts with the primary amines of proteins (i.a.) acting as an anchor that allows linkage to the swellable polyacrylamide hydrogel. Next, the sample is embedded in a monomer solution and polymerization of the gel is induced. After polymer synthesis and before expansion, the sample is homogenized by enzymatic digestion. Lastly, the addition of water expands the hydrogel. Created with Biorender.com.

Recently, for the first time, infected cells have been studied with ExM demonstrating the potential of this method to study viral proliferation in-depth. Intracellular membrane reorganization of SARS-CoV-2 infected cells in 3D has been captured (29). This ExM protocol increased the resolution so much that a comparison of vesicles between infected and non-infected cells was possible revealing that multivesicular bodies were enlarged upon infection. Moreover, specific proteins were visualized that indicated Golgi fragmentation. These findings highlight the valuable contribution of ExM to visualize viral infection.

Alternatively, advancements in microscope and software engineering have led to the development of super-resolution microscopes that do not require elaborate sample preparation. One new super-resolution method, referred to as SRM in this report, uses a modified spinning disk (SoRa spinning disk) and a compatible deconvolution software that allows optimal optical reassignment of the emitted photons to the center they originate from (30). Additionally, the use of immersion oil enables imaging with minimal spherical aberration (31). In combination, an effective resolution of approximately 100 nm can be achieved (30,32). In comparison to ExM, this method does not require extensive sample preparation and allows use in routine research.

Here, we exploit ExM and SRM to investigate their applicability to study ROs. We utilize two mutant viruses with either fluorescent or small tags on different viral proteins (mGreenLantern-2A CVB3 and Spot-3A CVB3). We aim to visualize the localization of 2A and 3A in detail at numerous time points during infection. We establish protocols for both tags in transfected cells before preceding to infected cells and compare both super-resolution techniques in terms of resolution and image quality. With this, we aim to contribute to the understanding of RO composition and formation and to aid in the development of antivirals against enteroviruses.

Results

ExM protocol optimization for EGFP-3A expressing cells

Expansion microscopy offers a new tool to elucidate high resolution details. This new technique is optimized depending on the visualization target (33–36). To find the best conditions for 4-fold expansion microscopy in virus-infected cells, we compared several published protocols and a protocol previously set up for EGFP-3A expressing cells (28,37,38).

Hela cells, approximately 70 % confluent, were transfected with an EGFP-3A containing plasmid and fixed at 16 h post transfection (p.t.) with 3.7 % PFA. Successful EGFP-3A transfection was confirmed by analyzing GFP signals using EVOS fluorescent imaging system. To observe EGFP signals after homogenization, the fluorophore has to be labeled with an additional booster. Two different boosters against EGFP were tested, an anti-EGFP nanobody conjugated to Atto488 and an anti-EGFP polyclonal antibody (pAB) together with an anti-rabbit antibody conjugated to AlexaFluor®488. Since both boosters work equally well (data not shown), we proceeded with anti-EGFP pAB. Samples were subjected to the aforementioned ExM protocols. The key differences among protocols are summarized in table 1 and can be found in the supplements.

Table 1: Differences between ExM protocols. Three ExM protocols named Raquel, Lukas and SDS were compared. Differences were the percentage of Triton-X-100, 0.1 % or 0.5 %, different blockage buffers, 2 % BSA and 0.1 % Saponin or 3 % BSA and the homogenization method, enzymatically with prot. K or chemically with SDS.

Protocol name	% Triton-X-100	Blocking Buffer	Homogenization solution
Raquel (37)	0.1	2 % BSA, 0.1 % Saponin	Enzymatic (8U/mL prot.K)
Lukas(28)	0.5	3 % BSA	Enzymatic (8U/mL prot.K)
SDS (39)	0.5	3 % BSA	Chemical (200 mM SDS)

During sample preparation, we encountered multiple difficulties such as uneven and inconsistent incorporation of the sample into the gel. This restricted the use of high magnification objectives (Fig. 3, middle panel) and resulted in a limited increase in resolution. First, the different concentrations of Triton-X-100 did not change the sample condition much. Second, the use of saponin, a detergent that allows reversible permeabilization, did not have any additional value in Raquel's protocol. Before saponin treatment, the cells were irreversibly permeabilized with Triton-X making the addition of saponin redundant. Lastly,

SDS-treated gels were larger and less firm than enzymatic-treated ones which made handling them more difficult. Therefore, we selected 0.5 % Triton-X-100, 3 % BSA and proteinase K (prot.K) treatment for our optimized 4x ExM protocol.

Olympus SoRaSpin10 system resolves tubular structures of EGFP-3A expressing cells

After optimizing the 4x ExM protocol, we compared the resolving power of ExM to SRM using Olympus SoRaSpin. As a proof of concept, EGFP-3A-expressing cells were subjected to ExM or SRM.

At lower magnification, signals obtained with SRM and ExM did not significantly differ from each other. However, by zooming into the cytoplasmic regions of the cells, one can distinguish differences in the signal intensities of 3A. For ExM, signals were weaker and dispersed through the cytoplasm (Fig. 3, middle and right panel). Whereas for SRM, EGFP signals were clearly recognizable visualizing 3A expression that was found as a tubule-like network (Fig. 3, left panel).

Furthermore, SRM was robust and reproducible in comparison to ExM. To exemplify the variations among ExM samples, two different experiments are shown in figure 3. The two experiments differed in the chosen homogenization treatment, one was chemically homogenized (Fig. 3, middle panel) and the other one enzymatically (Fig. 3, right panel). The two images differed in resolution and EGFP signal intensities. The samples were positioned at a distance that was too far away from the coverslips. This prohibited imaging with high numerical aperture objectives since they are limited in imaging depth, which is defined by the characteristic working distance of an objective. Hence, one ExM sample was imaged using a 20 x air and the other one using a 40 x air objective. None of the ExM samples could be imaged with the 60 x oil objective that was used for SRM. One factor that could influence the distance between the sample and the coverslip, is the incorporation of the sample into the gel. Another factor that most likely contributed to the variations between ExM samples was the deviating (degree of) gel expansion. A uniform expansion is determined by successful homogenization that depends on the treatment, which is chemical or enzymatic in this work (36). There were no disordered cells observed in either of the experiments. This indicates that the different treatments did not cause anisotropic irregularities that could be noted by the eye.

Yet, both ExM samples suffered from bleaching which reduced imaging depth (supplementary movie S1). SRM did not suffer from bleaching and the SoRaSpin system visualized the cellular tubular network of 3A at different focal planes. This allowed 3D reconstruction of 3A-expressing cells (supplementary movie S2).

Together, these results indicate that in comparison to ExM, SRM provides a robust method that did not suffer from sample variability and at the same time achieved similar resolution. Consequently, both ExM and SRM were further assessed to determine their applicability to infected samples.
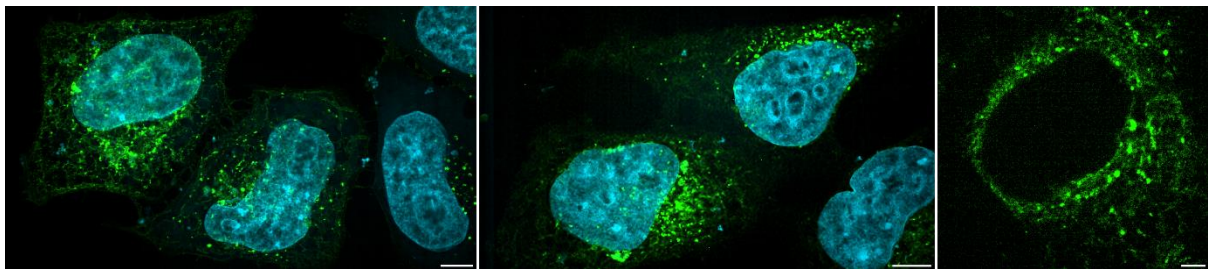

Figure 3: Resolving capacity of SRM vs. ExM. EGFP-3A expressing cells were fixed 16 h post transfection, EGFP signals were labeled using an anti-EGFP polyclonal antibody (green) and the nucleus was stained with DAPI (blue). All images were deconvolved. Left: Super-resolution microscopy images obtained using 60 x immersion oil objective. *The scale bar represents 5 μm.* Middle and right: Expansion microscopy was performed on two different samples. Middle: The sample was homogenized using SDS. ExM sample preparation limited the use of high magnification objectives. The image was acquired using a 20 x air objective (simultaneously prepared with SRM). *The scale bar represents 20 μm.* Right: Sample was homogenized using prot.K. ExM acquired with 40 x air objective (different data collection). The image was median filtered. *The scale bar represents 10 μm.*

mGL-2A CVB3 offers a new tool to visualize 2A localization

To investigate the localization of viral protease 2A, CVB3 was genetically modified to intrinsically label 2A by expression of a fluorescent protein, mGreenLantern (mGL). mGL was inserted at the N-terminus of 2A using the P1-IRES-P2-P3 platform (supplementary figure S1A). To determine that the addition of mGL at the N-terminal of 2A does not interfere with the localization and the function of 2A, we compared the localization of 2A in mGL-2A CVB3 infected cells to WT CVB3. Hela cells were infected with either CVB3 strain and fixed at 5 h post infection (p.i.). Cells were stained with an antibody against 2A and with DAPI against nuclei. Cells were imaged using Olympus SoRaSpin10 operating in confocal mode with 60 x oil objective.

We determined whether mGL insertion affects the localization of 2A. 2A was distributed throughout the cytoplasm in WT CVB3 and mGL-2A CVB3 (supplementary figure S1, a-2A channel). There were no significant differences in 2A localization between the different virus

strains. However, the WT CVB3 strain had lower 2A expression overall. Differences in expression levels of 2A within one sample showed cells at different stages of viral infection (data not shown). We conclude that the localization of 2A did not change due to fluorophore insertion. Then, the coincidence between 2A and mGL signals for each virus strain, WT and mGL-2A CVB3 respectively, was analyzed. For half of mGL-2A CVB3 infected cells, both signals were detected. Although the background signals of mGL are high, they are distinct from 2A. A few cells were 2A-positive and mGL-negative suggesting that mGL was either not yet expressed or that these cells were infected with CVB3 that counter-selected against mGL. We argue that the second reason is more likely since we would expect low signals if 2A expression was delayed (40). Together, these results demonstrate that mGL is specific for 2A.

Additionally, we examined whether the use of an additional booster, that is required for ExM protocol, introduces artifacts. mGL signals were boosted using an anti-EGFP pAB and anti-rabbit Alexa488and compared to mGL-2A CVB3 infected cells that were not boosted. In comparison to the unboosted sample, the booster slightly increased the signal intensity of mGL indicated by larger signal differences between cells (supplementary figure S1). GalT-GFP expressing cells were used as a negative control. Hela cells were transfected using a GalT-GFP containing plasmid, fixed at 16 h p.t. and labeled as described for mGL-2A infected samples. Comparable to mGL-2A infected cells, no changes in GFP localization between boosted and unboosted samples were observed in GalT-GFP expressing cells (supplementary figure S2). This confirms that the booster introduced no visible labeling artifacts.

In-depth visualization of 2A using SoRaSpin SRM

After confirmation that neither mGL expression nor the use of a booster introduces any artifacts, mGL-2A CVB3 infected cells were subjected to ExM and SRM. Infected cells were fixed at 5 h p.i. using 3.7 % PFA supplemented with 4 % sucrose to ensure fixation in a more gentle manner (29). EVOS fluorescent imaging system was used to confirm mGL signals after fixation. For our data collections in super-resolution mode, we have chosen high-expressing cells, like the two cells observed in the boosted sample (supplementary figure S1B). High-expressing cells are easier to image since high signal intensities do not need high laser power and thus the S/N noise will be reduced.

Unexpectedly, the signal intensity of mGL-2A in expanded samples was very low (Fig. 4B). Therefore it is not clear if the obtained signals correspond to 2A or if they are merely

background noise. In another experiment, we stained mGL-2A CVB3 infected samples against 2A. However, it was not possible to colocalize mGL with the immunofluorescent signals from the anti-2A antibody as the signals were too low for detection with ExM (data not shown). On the contrary, the localization of 2A was successfully visualized in-depth using SRM which could capture details that were not resolved using a conventional confocal microscope (Fig. 4C and supplementary figure S1). mGL-2A was abundantly located as clusters throughout the cytoplasm yet more in the perinuclear region. Interestingly, these clusters consisted of numerous dots in different sizes (Fig. 4C). In conclusion, SRM provided more insights into the localization of the viral protein than ExM without the risk of imaging noise.
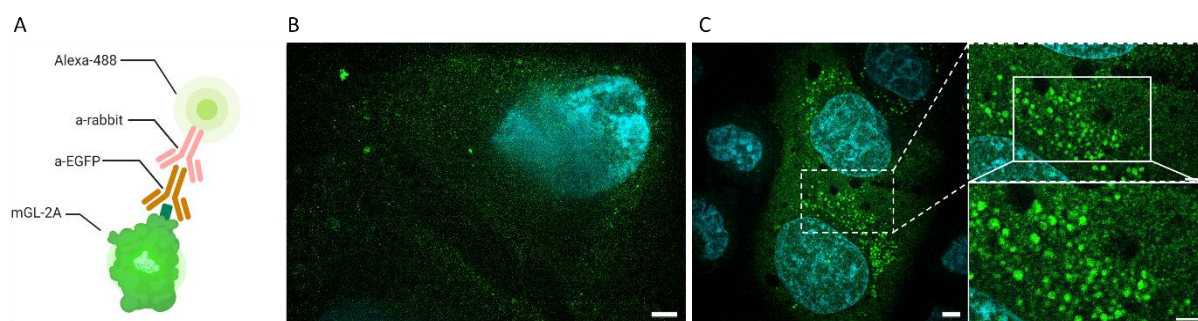

Figure 4: Comparison of ExM and SRM for mGL-2A CVB3 infected samples. A: Immunofluorescence labeling of mGL-2A. mGL was labeled with anti-EGFP polyclonal antibody and anti-rabbit antibody conjugated to AlexaFluor®488. B, C: Expansion microscopy (B) and super-resolution microscopy (C) on mGL-2A CVB3 infected cells at 5 h p.i., labeled as illustrated in A. mGL (green) and stained with DAPI (blue). Images were acquired with SoRaSpin10 Olympus operating in SR mode using 60 x oil objective. *Scale bars represent 5 μm and 2 μm (zoom-in).*

2A does not localize at replication sites

Since SRM could be used to reveal the localization of viral protease 2A in detail, we further investigated how 2A localization would change over the course of infection using SRM. mGL-2A CVB3 infected cells were fixed at different time points, 3 to 6 h p.i. (Fig. 5 and 6). Over the course of infection, 2A signals increased and spread in the cytoplasm indicating active replication. 2A did not localize at one specific site which was expected since it does not have any transmembrane domain to target specific cellular organelles (20). Early in infection (3 h p.i.), 2A signals were identified as dot-like clusters that differed in size. Most clusters were small. At 4 h p.i. and later, these clusters accumulated in the cytoplasm. The clusters did not significantly grow in size, but quantity. The expression pattern was changed late in infection when 2A was highly expressed. At 6 h p.i., 2A signals were intense and distributed throughout the entire cellular environment including the nuclear region. 2A clusters were overlaying

making distinguishment from each other difficult; contrary to the clusters observed early in infection.

2A might be involved in RO composition by mediating the translocation of the key enzyme of PC synthesis from the nucleus to the cytoplasm where it can interact with the membranes of ROs. To examine if 2A is found at replication sites, we investigated the coincidence of mGL-2A with either viral protein 3A or host protein PI4KB as RO markers. 2A did not immediately localize to ROs. At later time points, 2A coincides with RO markers. However, no further conclusions could be drawn as the overlapping signals were most likely a result of high protein levels due to progressed viral proliferation.
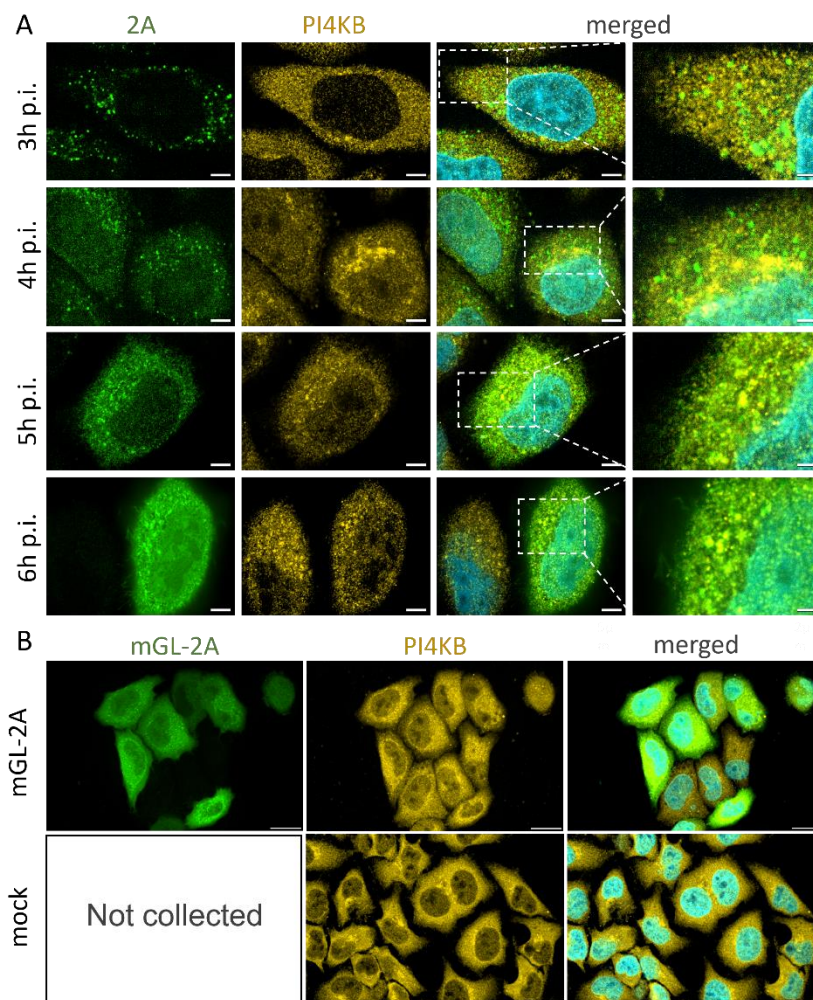

Figure 5: Colocalization of 2A with RO marker PI4KB. A: mGL-2A infected cells were fixed 3 h, 4 h, 5 h and 6 h p.i., mGL signals were additionally boosted with anti-EGFP pAB (green). All samples were stained against PI4KB (yellow) and with DAPI (blue). Images were acquired with SoRaSpin10 Olympus operating in SR mode using 60 x oil objective. *Scale bars represent 5 µm or 2 µm (zoom-in).* B: mGL-2A infected cells at 5 h p.i. and mock (uninfected cells) were stained against PI4KB (yellow) and nucleus (blue). Images were acquired with SoRaSpin10 Olympus operating in SR mode using 60 x oil objective. *Scale bars represent 20 µm.*
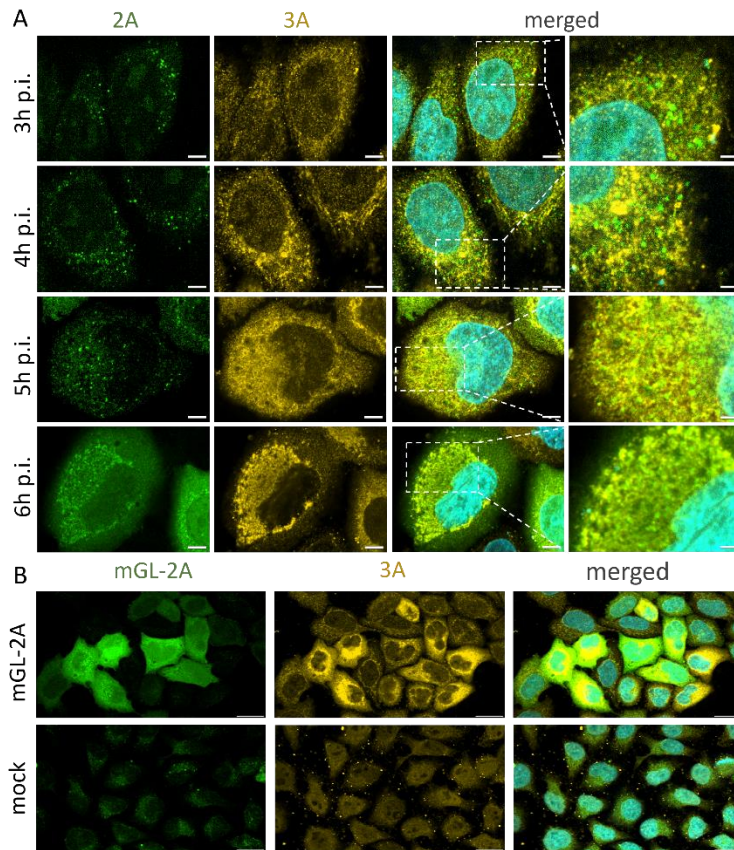
Figure 6: Colocalization of 2A with RO marker 3A. A: mGL-2A infected cells were fixed 3 h, 4 h, 5 h and 6 h p.i., mGL signals were additionally boosted with anti-EGFP pAB (green). All samples were stained against 3A (yellow) and with DAPI (blue). Images were acquired with SoRaSpin10 Olympus operating in SR mode using 60 x oil objective. *Scale bars represent 5 µm or 2 µm (zoom-in).* B: mGL-2A infected cells at 5 h p.i. and mock (uninfected cells) were stained against 3A (yellow) and nucleus (blue). Images were acquired with SoRaSpin10 Olympus operating in SR mode using 60 x oil objective. *Scale bars represent 20 µm.*

Spot-tag labels enterovirus 3A protein

Replication organelles have been previously studied using the viral protein 3A as a marker. This membrane-associated protein is involved in virus-induced membrane rearrangements and localizes at viral replication sites (11,25,37,41). By targeting 3A, we can study how ROs evolve over time and at what time points 3A interacts with host factors in the context of changes in RO structure. Contrary to 2A, 3A cannot easily be labeled using EGFP without changing its conformation. Consequently, 3A was labeled with the Spot-tag, a 12 amino acids (aa) long peptide, inserted after the first two amino acids of 3A (Fig. 7A) (42–44).

To validate that the Spot-tag does not change the localization of 3A, we compared the genetically modified CVB3 strain to WT CVB3 (Fig. 7B). Hela cells were infected with Spot-3A CVB3 or WT CVB3 and fixed at 5 h p.i. with 3.7 % PFA. Both samples were stained with an antibody against 3A and the Spot-nanobody conjugated to AlexaFluor488 against the Spot-tag. Images were taken with Olympus SoRaSpin10 operating in confocal mode using 60 x oil objective. The antibody labeling against 3A suggested a slightly higher infection rate for Spot-3A CVB3, but the intensity levels of infected cells were similar among both virus strains. The merged image of Spot-3A CVB3 infected cells showed a coincidence of anti-3A and Spot-tag-

3A labeling, apparent as yellow signals. In contrast to WT CVB3 infected cells, where the merged signals originated from the antibody labeling solely, indicated by red signals. This observation suggested that the Spot-tag is specific for 3A. SR images did not show a clear coincidence between the 3A antibody and Spot-3A (supplementary figure S3). This could be explained by the antibody that was used. It binds to the first 60 aa of 3A, the sequence in which the Spot-tag was inserted.
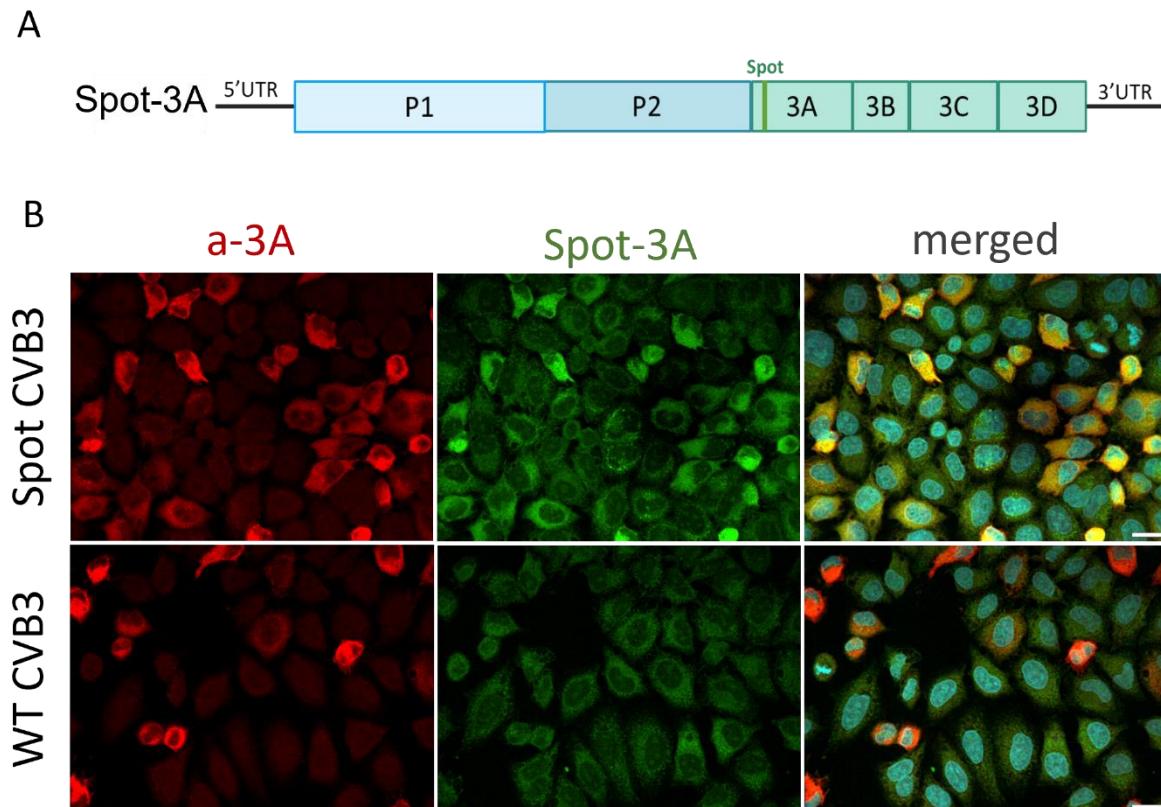

Figure 7: Validation of Spot-3A signals. A: Viral genome of Spot-3A CVB3. Spot-tag was inserted after the first two amino acids of 3A. B: Spot-3A and 3A-WT CVB3 infected cells were fixed at 5 h p.i. Cells were stained with an antibody against 3A (red) and the Spot-nanobody against the Spot-tag (green). Nuclei were stained with DAPI (blue). Images were acquired with SoRaSpin10 Olympus operating in confocal mode using 60 x oil objective. *Scale bars represent 20 µm.*

In-depth visualization of 3A using SoRaSpin SRM

After we confirmed that the Spot-tag did not alter 3A localization, we performed ExM on Spot-3A expressing cells to establish a working ExM protocol for this tag before proceeding to infected samples. Unlike for mGL-2A, there was no ExM protocol that had been previously optimized for the Spot-tag. As SRM was shown to be a promising technique to localize EGFP-3A, SRM was performed in parallel to ExM. Hela cells were transfected with a plasmid containing Spot-3A and fixed at 16 h p.t. Fixed cells were stained with Spot-nanobody conjugated to AlexaFluor488 against Spot-tag according to the manufacturer's protocol.

Successful staining of Spot-tag was confirmed using EVOS fluorescent imaging system. Samples were either directly mounted on coverslips for SRM or taken further for the ExM procedure. We captured high resolution details of 3A with ExM and SRM (Fig. 8). However, only SRM revealed the tubule-like network that has been observed for EGFP-3A expressing cells (Fig. 3). Comparing both techniques, our data showed better spatial distribution and higher signal intensities for SRM. Moreover, a higher resolution was achieved using SRM (supplementary figure S4). Together, we demonstrated the feasibility of the Spot-tag for both super-resolution microscopy techniques.
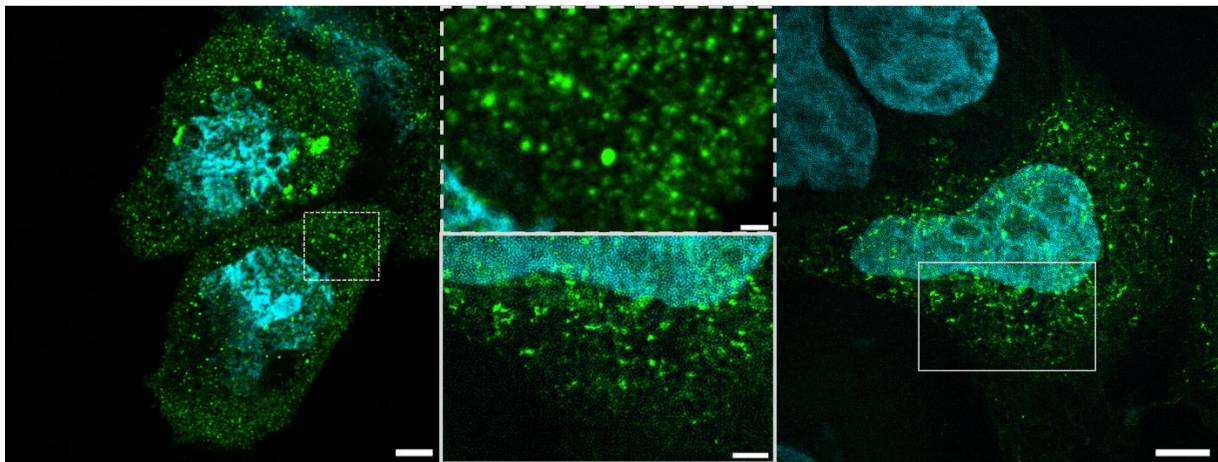

Figure 8: Comparison of ExM and SRM. Spot-3A expressing cells were stained with Spot-nanobody conjugated to AlexaFluor488 (green) and with DAPI (blue). Images were acquired with SoRaSpin10 Olympus operating in confocal mode (ExM, left) and in SR mode (SRM, right) using 60 x oil objective. *Scale bars represent 10 μm and 2 μm (ExM) and 5 μm and 2 μm (SRM).*

Localization of 3A in infected cells at early time points

As SRM achieved higher resolution than ExM, we used this method to study 3A localization in infected cells. Spot-3A CVB3 infected cells were stained using Spot-nanobody conjugated to AlexaFluor488, fixed at different time points and imaged using Olympus SoRaSpin10 operating in SR mode. In comparison to the signals obtained by immunofluorescent staining against 3A (Fig. 6A), better results were obtained using the Spot-tag. The combination of SRM and Spot-labeling offered the possibility to obtain high resolution details of 3A in infected cells (Fig. 9). In comparison to the signals obtained by immunofluorescent staining against 3A, which were too weak and thus limiting the use of additional microlenses that are required to perform super-resolution microscopy, Spot signals were clearly visualized. SRM captured clearly distinguishable signals of the viral protein while with conventional confocal microscopy the resolution was too poor to resolve molecular details (Fig. 7B).

In infected cells, 3A formed spherical clusters of similar size that were observed throughout the cell but accumulated proximal to the nucleus. These perinuclear clusters were visible at different time points (supplementary figure S5) which is in agreement with previous studies (42,45). The brightness of the Spot-nanobody enabled imaging of 3A at low expression, i.e. early in infection. Thus, we were able to detect 3A at 3 h p.i. Already early in infection, 3A showed its characteristic perinuclear localization (Fig. 9). Our data suggest that imaging at earlier time points might be possible due to the clear signal detection of Spot-3A at 3 h p.i. (Fig. 9).

At last, we showed that SRM can be used to visualize host proteins, i.e. PI4KB and ACBD3, that localize at RO membranes. ACBD3 mediates the interaction between 3A and PI4KB (11–13). Spot-3A CVB3 infected cells were fixed at 5 h p.i. and stained against the Spot-tag and PI4KB or ACBD3. As expected from the literature, ACBD3 and PI4KB were both located proximal to the nucleus, close to 3A (supplementary figure S6). A coincidence between 3A and ACBD3 or PI4KB was observed for low intensity signals, however high intensity signals did not clearly coincide. This finding suggests that these proteins accumulate in different regions at the RO membranes. Altogether, SRM allowed us to study the distribution of RO markers and investigate their colocalization.
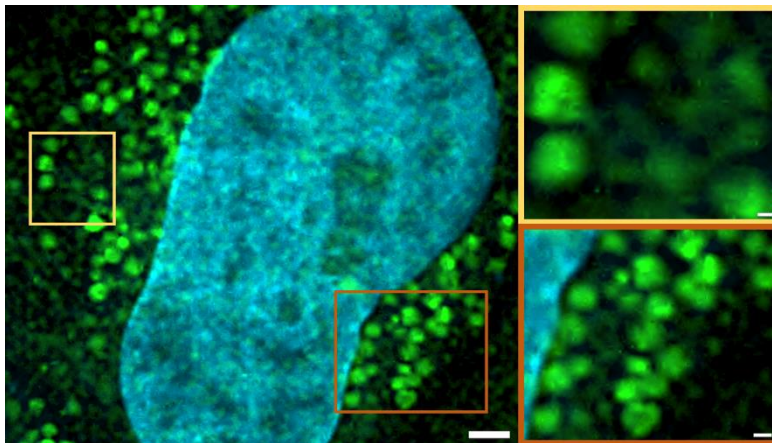

Figure 9: SRM on Spot-3A CVB3 infected cells. Hela cells were infected with Spot-3A. Spot-tag was labeled with Spot-nanobody conjugated to AlexaFluor488. Cells were fixed at 3 h p.i. against 3A (green) and with DAPI (blue). Images were collected with Olympus SpinSR10 operating in SR mode, 60 x oil objective. *Scale bars represent 2 µm, 500 nm and 200 nm.*

Discussion

Upon infection, enteroviruses cause rearrangements of host cell endomembranes which leads to the formation of compositionally unique platforms, so-called replication organelles (ROs) that facilitate efficient viral replication. To study viral components involved in RO formation and their interaction with the cellular environment, high resolution data is required.

We have established ExM protocols for two labels, EGFP and Spot-tag in transfected cells. Due to the high sequence similarity between EGFP and mGL, the established protocol for EGFP can be used interchangeably for mGL (40). In comparison to other fluorophores, mGL is 620 % brighter than EGFP and its fluorescence develops 4 times faster than EYFP (33). However, the protein is too big to be inserted into the viral genome without additional modifications. This restricts its applicability to all viral proteins. Contrary, the Spot-tag is small (12 aa), but not fluorescent by itself. It is recognized by the bivalent Spot-nanobody which is conjugated to Alexa Fluor® 488, the brightest and most photostable green dye (46).

ExM sample quality varied among samples. This variation can be explained by uneven and inconsistent incorporation of the sample into the gel. The use of a gelation chamber can be advantageous to improve sample quality (28,33,34). It provides a platform for even gel formation. Moreover, the gelation chamber allows easy transfer of the gel, which is stuck on the coverslip, to the petri dish, where it will be expanded. Another tool that facilitates the handling of the gel is a self-printed imaging chamber as suggested by Jurriens and colleagues (33). The gel can be transferred from the petri dish into the chamber without the need of additional utensils, e.g. razor blades.

In Spot-3A and EGFP-3A expressing cells, ExM revealed 3A positive membrane structures in detail (Fig. 3 and 8). Despite the excellent qualities for imaging, we could not establish a working ExM protocol for either label in infected cells. So far, ExM has been mostly used to study highly abundant structures in the cell, like microtubules (33). Studying less abundant proteins is challenging due to the reduced signal intensity in expanded samples. Moreover, infection reduces the cellular integrity which might cause problems in the expansion procedure (47). To date, there are only a few studies that have shown ExM on infected cells

targeting abundant proteins (29,35,48,49). These studies suggest that 2A and 3A could be visualized when expression levels are high, e.g. at 5 h p.i.

Infected samples suffered from low signal detection (Fig. 5 and 9). For infected cells, we have exploited prot. K because the handling of these gels was easier than SDS-treated gels. However, prot. K cleaves peptide bonds with low specificity resulting in the formation of small peptides. These small peptides can diffuse through the reticulation of the hydrogel which might be an explanation for why our samples suffered from a low amount of signals. Alternatively, SDS leads to protein unfolding without disruption of the primary structure (36). We have established a protocol for transfected cells using SDS as a homogenization agent. Thus, we suggest applying this protocol to infected cells as the use of SDS might increase the low signals. Another suggestion to increase the signal is the use of cryofixation. Cryofixation has been recently combined with ExM and showed an increase in the labeling efficiency of epitopes while preserving the native ultrastructure of the cells (50).

We have visualized the localization of two viral proteins, 2A and 3A, over the time course of infection in detail using the Olympus SoRaSpin10 system. This system does not require extensive sample pre-treatment like ExM. Our data is the first evidence of 2A localization. 2A was abundantly located as clusters throughout the cytoplasm yet more in perinuclear regions. However, whether 2A is associated with RO membranes remains unclear. The observed coincidence between 2A and 3A or PI4KB, two proteins that serve as markers for ROs, was not significant. Our data suggested that 2A is not directly located at ROs. Consequently, visualization of other RO markers, viral RNA or lipids, might shed light on the role of 2A in RO formation.

For 3A, our data confirmed the perinuclear localization of this viral protein and suggest the presence of dispersed peripheral RO foci which are said to interact with ER (11,25). To validate the proposed interaction, colocalization with ER has to be examined. Our data of other RO markers, i.e. ACBD3 and PI4KB, suggested that ACBD3, PI4KB and 3A accumulate at different sites at the RO membrane. However, to study their distribution during RO formation, these proteins have to be visualized within one sample and at different time points during viral infection.

We showed that Spot-labeling is better suited for SRM than anti-3A staining (supplementary figure S3). Furthermore, we can assume that due to Spot-labeling, the localization of 3A is more accurately represented. The linkage error, i.e. the error caused by the displacement of the signal due to the size of the label, for antibodies is approximately 30 nm. However, as the nanobody that binds to the Spot-tag is directly bound to a fluorescent dye, this error is reduced to 8 nm (51). For the first time, 3A was detected at 3 h p.i. Our approach, i.e. SRM combined with Spot-labeling allows visualization of viral proteins in better resolution at early time points and offers an alternative to tag a protein that has no available antibody. However, the Spot-tag is only feasible for fixed samples and thus cannot be used for live-cell imaging.

One disadvantage of the Olympus SoRaSpin10 system is the high background noise (Fig. 7, mock). This might be problematic for samples with low signal intensities (Fig. 5, ExM) as the risk of image noise is increased. Longer exposure time and higher laser power can improve the S/N ratio. At the same time, to reduce the bleaching by the increased laser power, an anti-quencher can be used (52). Alternatively, the Olympus imaging software allows automatic subtraction of previously recorded background noise of the sample.

In comparison to other super-resolution microscopy techniques, e.g. stochastic optical reconstruction microscopy (STORM), photoactivated localization microscopy (PALM) and stimulated emission depletion (STED) microscopy, the Olympus system uses the same sample preparation protocols as conventional confocal microscopy and does not require extra materials. Hence, neither extensive sample preparation nor long protocol optimization is required, making this system time-efficient and straightforward to use. Furthermore, the Olympus SpinSR10 system offers the possibility to combine SRM with live-cell imaging. Thus, tracking of viral protein localization, RO formation and its dynamics could be further investigated.

To further increase the resolution that we have achieved in this study, SRM can be combined with our established ExM protocols. Moreover, other ExM protocols that offer greater expansion, e.g. 10 x ExM and 20 x ExM can be used alternatively to our 4 x ExM protocol (28,39).

Altogether, these data demonstrate that super-resolution microscopy using the Olympus® SpinSR10 system provides high resolution details and allows localization of viral proteins over

the time course of infection. The resolution can be further improved upon the combination of ExM and SRM. Another possibility is to combine SRM and live-cell imaging. This might elucidate the importance of various host factors, that have been reported to facilitate enteroviral replication and their associations with viral proteins concerning RO formation and composition. Ultimately, a comprehensive understanding of the functioning of replication organelles can lead to the design of anti-viral drugs to impede virus replication.

Materials and methods

Key resources table

Reagent or resource	Source	Identifier
Antibodies & nanobodies		
Rabbit anti-EGFP (pAB)	UU-Virology (53)	
V$_H$H anti-EGFP conjugated to ATTO488	Chromotek	
Rabbit anti-3A (CVB3 1-60, pAB)	In house	
Rat anti-2A	Gift from Malin Flodström-Tullberg	
Rabbit anti-PI4KB (pAB)	MERCK	#06-578
Anti-Spot-Tag®VHH (bivalent)	Chromotek	AB_2889374
Rabbit anti-VHH	QVQ	QE19
Goat anti-rabbit IgG Alexa594	Invitrogen	A11012
Goat anti-rat IgG (H+L) AlexaFluor®555	Invitrogen	A21434
Goat anti-rabbit IgG (H+L) AlexaFluor®488	Invitrogen	A11034
Streptavidin, Alexa Fluor™ 647 conjugate	Invitrogen	S21374
Chemicals, dyes, protein stains		
PBS	Lonza	17-512F
APS	Sigma Aldrich	A3678
TEMED	SERVA	35925
Poly-L-lysine	Sigma Aldrich	P8920
ProLong™ Diamond	Invitrogen	P36961
DAPI	Invitrogen	D21490

Biotinylated Wheat Germ Agglutinin (WGA)	Vector Laboratories (conc: 10 mg/mL)	B-1025
Proteinase K	Thermo Fisher Scientific	EO0491
Acryloyl X-SE	Thermo Fisher Scientific	A20770
Cell line		
Hela R19	G. Belov (University of Maryland and Virginia-Maryland Regional College of Veterinary Medicine, US)	
Virus strains		
I-1031 - pRibCB3_T7-3A (SPOT aa2) p2	UU-Virology	
I-923 pRibCB3/T7 P1-IRES_EMCV-P2-P3 p1	UU-Virology	
I-1028 - pRibCB3_T7 P1-IRES_EMCV-mGreenLantern-P2-P3	UU-Virology	
CVB3 WT Nancy	UU-Virology	
Recombinant DNA		
P3081 3A-Spot tag	UU-Virology	pCMV-3A (Spot aa2)
EGFP-3A	UU-Virology	pACT-EGFP-3A
pEGFP-GalT	A gift from Jennifer Lippincott-Schwartz (Addgene plasmid 11929)	pCMV-GalT(EGFP)
Software		
Olyvia	Olympus	https://olyvia.software.informer.com/versions/
Biorender	Biorender	https://biorender.com/
Other		

10 mm precision coverslips, thickness No. 1,5H	Marienfeld	Cat# 0117500
25 mm coverslips, thickness No. 1,5H	VWR International	Cat# 631-0172
4-well plate	Thermo Fisher Scientific	Cat# 144444
Attofluor™ cell chamber	Thermo Fisher Scientific	A7816

Cells

Hela R19 cells were maintained in Dulbecco's modified Eagle's medium (DMEM, LONZA) supplemented with 10 % fetal calf serum (FCS) growing at 37°C in 5 % CO_2.

Viruses and infections

For infections CVB3 WT, CVB3 IRES WT, CVB3 mGL-2A and CVB3 Spot-3A were used.

Hela cells were seeded the day prior to infection on 10 mm coverslips (Marienfeld) in a 4-well plate (Thermo Fisher Scientific) and grown until a confluence of approximately 90 %. Viruses were inoculated at the multiplicity of infection (MOI) of 10 for 30 minutes at 37°C in 5 % CO_2. After inoculation, viruses were removed and fresh DMEM was applied. The cells were grown until fixation; 3h, 4h, 5h or 6h post infection.

Plasmids and transfections

For transfections EGFP-3A, GalT-GFP or Spot-3A containing plasmids were used.

Hela cells were seeded the day prior to transfection on 10 mm coverslips in a 4-well plate and grown until a confluence of approximately 70 %. 500 ng of plasmid DNA and Lipofectamine 2000 (Thermo Fisher Scientific) was combined in Opti-MEM (Thermo Fisher Scientific), mixed and incubated for 20 minutes at room temperature (RT) before adding to Hela R19 cells. The cells were grown until fixation 24h post transfection.

Fixation

Before fixation, Hela R19 were washed once with 1x PBS (LONZA). Transfected cells were fixed with 3.7 % paraformaldehyde (PFA, Merck, 104003) in 1x PBS (w/v) and infected cells were

fixed with prewarmed 3.7 % PFA supplemented with 4 % sucrose in 1x PBS (w/v, w/v) for 10 minutes at RT. Fixed samples were stored in 0.5 % PFA in 1x PBS (w/v) at 4°C or directly taken for immunofluorescence staining.

Immunofluorescence staining of fixed samples

Spot-3A transfected or infected samples were washed once with 1x PBS and then permeabilized with 0.5 % Triton-X-100 in 1x PBS for 5 minutes. After 2x washing steps with 1x PBS, cells were blocked in 4 % bovine serum albumin (BSA, Biovit) in 1x PBS for 10 minutes at RT. Samples were incubated with primary antibodies and Spot-V_HH for 45 minutes at RT. After 3x washing in 1x PBS, samples were incubated with corresponding secondary antibodies and DAPI in 4 % BSA for 45 minutes at RT.

For any other infection or transfection, samples were washed once with 1x PBS and permeabilized with 0.1 % Triton-X-100 in 1x PBS for 15 minutes at RT. Primary and corresponding secondary antibodies were prepared in 2 % normal goat serum. Samples were incubated for 45 minutes at RT and washed in between antibody stainings three times with 1x PBS.

Before mounting, all samples were 3x washed with 1x PBS and once briefly with ddH$_2$O. Cells were mounted in Prolong Diamond (Invitrogen).

For expanded samples, cells were washed 3x with 1x PBS and permeabilized with 0.5 % Triton-X-100 in 1x PBS for 15 minutes. After 2x washing steps with 1xPBS, cells were blocked with 3 % BSA in 1x PBS for 15 minutes at RT. Primary, WGA staining and secondary antibodies were diluted in 4 % BSA in 1x PBS. Samples were incubated with primary antibodies for 2h at RT, washed 3x for 5 minutes with 4 % BSA and incubated with secondary antibodies for 2h at RT. Samples were washed twice with 1x PBS before the expansion procedure.

Antibodies

Primary antibodies in this study used were rabbit anti-3A (1:100), rat anti-2A (1:100), rabbit anti-VHH (1:500, QVQ), rabbit anti-PI4KB (1:50, MERCK) and anti-WGA-Biotin (1:50, vector laboratories). Spot-tag was detected using Spot-V_HH conjugated to AlexaFluor®488 (1:800, Chromotek) and GFP signals were boosted using anti-EGFP conjugated to Alexa488 (1:100, PRODUCER). Secondary antibodies used were Goat anti-rabbit IgG AlexaFluor®488 (1:80, Invitrogen), goat a-rat IgG conjugated to AlexaFluor®555 (1:400, Invitrogen), goat a-rabbit IgG

conjugated to Alexa594 (1:400, Invitrogen), streptavidin-AlexaFluor647 (1:200, Invitrogen) and DAPI (Invitrogen).

Expansion procedure

After labeling, samples were post-fixed with 0.1 mg/mL acryloyl X-SE (Thermo Fisher Scientific) in 1x PBS overnight (O/N) at RT. For gelation, a monomer solution was prepared containing 0.91 M sodium acrylate, 0.35 M acrylamide, 2 M NaCl and 0.0097 % N,N'-methylenebisacrylamide in 1x PBS. Gelation of the monomer solution was initiated with 0.08 % ammonium persulfate (APS) and 0.08 % tetramethylethylenediamine (TEMED). 40 µL of gelation solution were directly pipetted on a cold parafilm-covered metal plate. Coverslips were placed on the droplet, cells facing down and the sample was directly transferred to a 37°C incubator for 1 h to polymerize. After polymerization, gels were transferred to petri dishes and digested in digestion buffer (0.5 % Triton-X-100, 1 mM EDTA, 50 mM Tris (pH=8) and 0.8 M NaCl in ddH$_2$O) supplemented with proteinase K (8U/mL) O/N at RT. Post homogenization, gels were stained with streptavidin-Alexa647 (1:200) and DAPI in 1x PBS for 1 h at RT. For expansion, gels were transferred to petri dishes, and PBS was exchanged for ddH$_2$O. Then washed twice after 30 minutes with ddH$_2$O. Samples were left in ddH$_2$O to expand overnight.

For gel mounting, 50 mm coverslips (VWR International) were cleaned by O/N storage in EtOH, HCl solution before coating with poly-L-lysine (Sigma Aldrich). Poly-L-lysine coated coverslip was inserted in the Attofluor^{TM} cell chamber (Thermo Fisher Scientific). Gel size was adjusted to the cell chamber before mounting. The gel (cells facing towards the coverslip) was mounted using a customized 3D printed mould (CCI UU), water was added and the chamber was closed with a second coverslip.

Image acquisition and analysis

EVOS imaging

Before immunofluorescence staining and after the addition of Spot-nanobodies, GFP/mGL/EGFP signals were confirmed using the EVOS imaging system (Thermo Scientific, the Netherlands).

Confocal and super-resolution imaging of expanded and non-expanded samples

Imaging was performed on Olympus® SpinSR10 operating in confocal and SR mode (Evident, Netherlands, Leidendorp). SoRa disk was inserted and UPLXAPO 4 x (NA 0.16), UPLXAPO 20 x (NA 0.8), UPLXAPO 40 x (NA 0.95), UPLXAPO 40 xO (NA 1.4) and UPLXAPO 60 XOHR (NA 1.5) objectives were used.

Spatial distribution of signal intensities

Profile plots were generated using Fiji (54). One focal plane was chosen and a line was drawn manually proximal to the nucleus. The plots were recreated using Excel, the gray value was plotted against the distance (μm).

Supplements

A detailed protocol for ExM and SR is available: https://solisservices-my.sharepoint.com/:w:/r/personal/a_schlemmer_students_uu_nl/Documents/methods_protocol.docx?d=w5302bbc4c08e49929ebec8168b531837&csf=1&web=1&e=vfcJwB
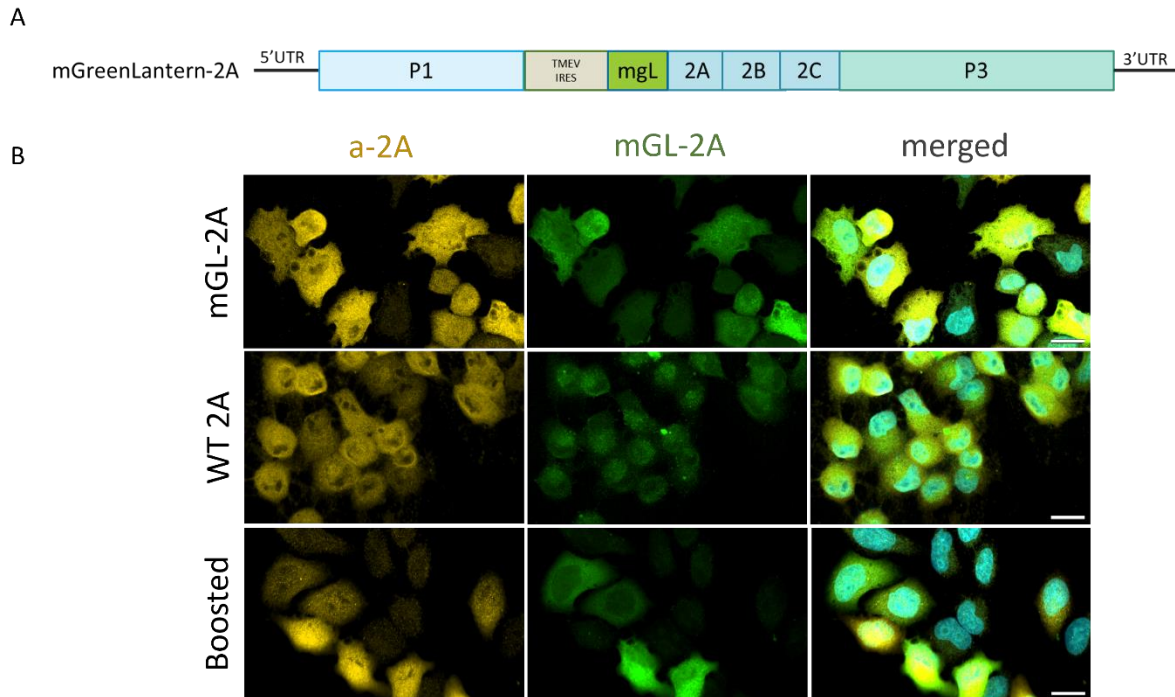
Supplementary figures

Figure S1: Validation of mGL-2A signals. A: Viral genome of mGL-2A CVB3. mGreenLantern was inserted, with an additional IRES at its N-terminus, at the N-terminus of 2A. B: Hela cells were infected with mGL-2A CVB3 (unboosted) or 2A-WT CVB3 (2A-WT) and fixed at 5 h p.i., mGL signals were additionally incubated with anti-EGFP pAB (boosted). All samples were stained against 2A (yellow) and with DAPI (blue). Images were acquired with SoRaSpin10 Olympus operating in confocal mode using 60 x oil objective. *Scale bars represent 20 μm.*
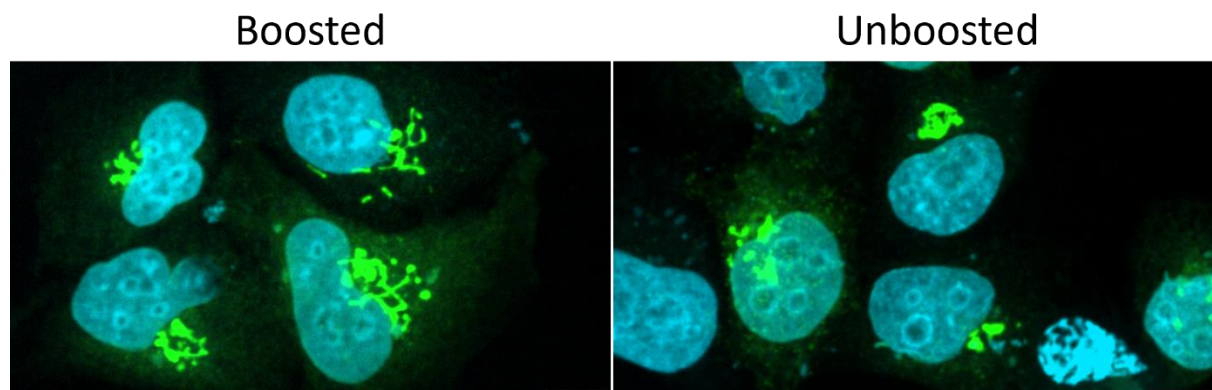

Figure S2: Negative control for mGL-2A boosted. GalT-GFP expressing cells were fixed at 16 h p.t. and stained against EGFP and rabbit antibody conjugated to AlexaFluor488 (boosted) or left unboosted. Images were acquired using Olympus SRSpin10 operating in confocal mode. Images were not deconvolved. *Scale bars represent 10 μm.*
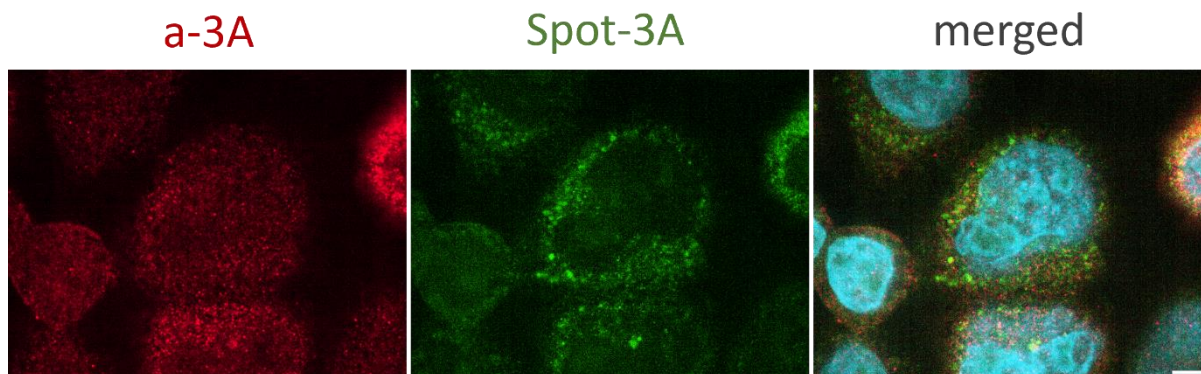
28

Figure S3: Co-staining of 3A on Spot-3A infected cells. Cells were fixed at 5 h p.i. and were stained against Spot-tag (green) and anti-3A (red). Images were acquired with SoRaSpin10 Olympus operating in SR mode using 60 x oil objective. *The scale bar represents 2 µm.*
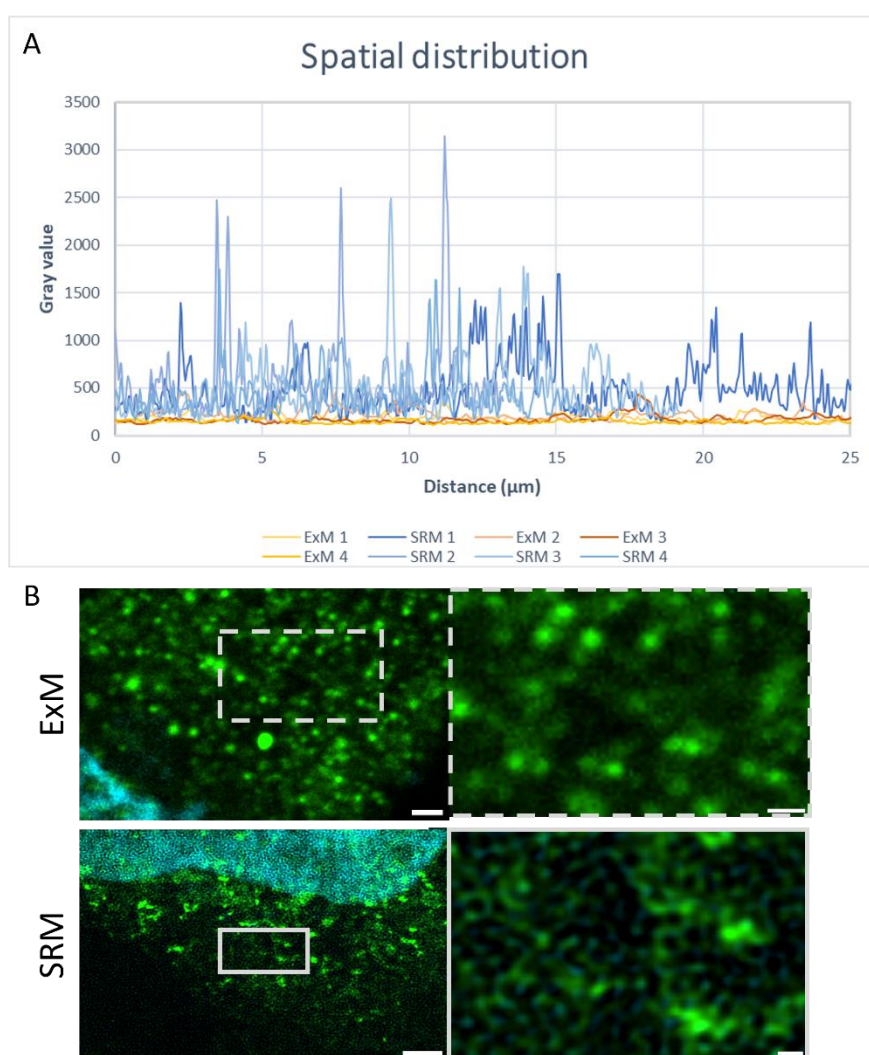

Figure S4: Comparison of ExM and SRM (spatial distribution and resolution). A: Spatial distribution of Spot-3A signals. The gray value of the Spot-3A channel was plotted against the measured distance (µm) using Excel. Measurements were performed in Fiji (N=1, n=4). B: Spot-3A expressing cells were stained with Spot-nanobody conjugated to AlexaFluor488 (green) and with DAPI (blue). Images were acquired with SoRaSpin10 Olympus operating in confocal mode (ExM, top) and SR mode (SRM, bottom) using a 60 x oil objective. *Scale bars represent 2 µm and 1 µm (ExM) and 2 µm and 200 nm (SRM).*
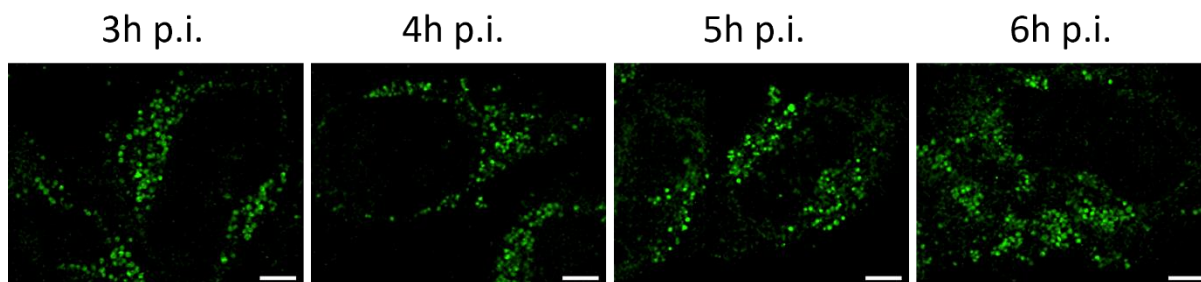
Figure S5: 3A signals of Spot-3A CVB3 infected cells. Spot-3A infected cells were fixed at 3 h, 4 h, 5 h and 6 h p.i. All samples were stained against Spot-tag (green). Images were acquired with SoRaSpin10 Olympus operating in SR mode using 60 x oil objective. *Scale bars represent 5 µm.*
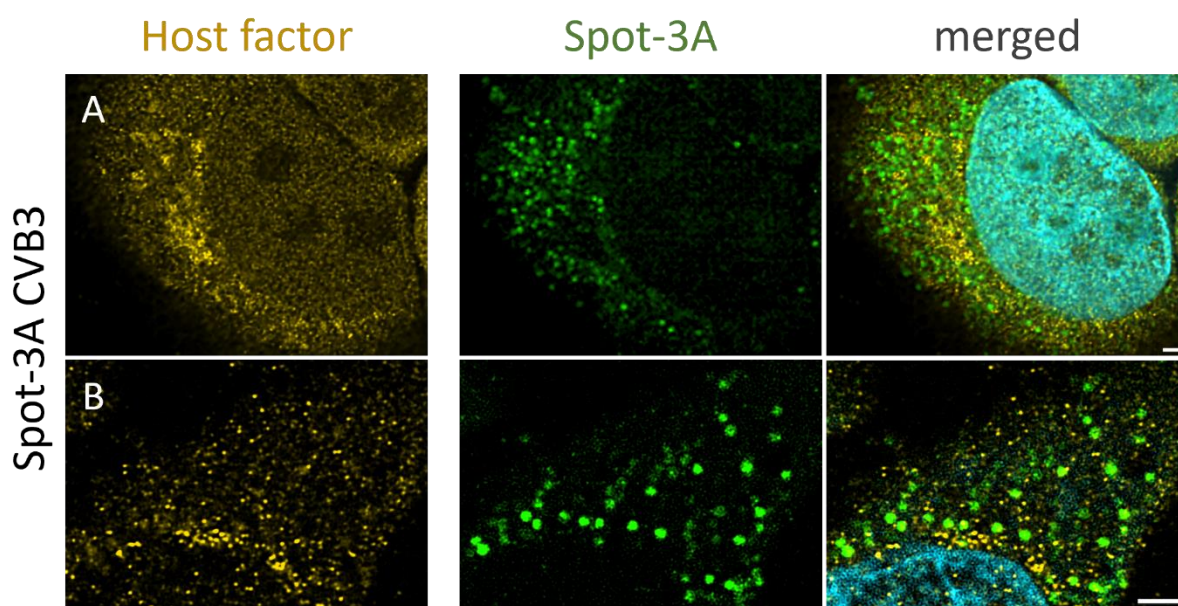

Figure S6: Colocalization of 3A and selected host factor. Spot-3A CVB3 infected cells at 5 h p.i. were stained against PI4KB (A) or ACBD3 (B) (yellow), Spot-tag (green) and the nucleus (blue). Images were acquired with SoRaSpin10 Olympus operating in SR mode using 60 x oil objective. *Scale bars represent 2 µm.*

Movie S1: Fast bleaching of expanded cells

https://solisservices-my.sharepoint.com/:v:/r/personal/a_schlemmer_students_uu_nl/Documents/20220114_AS05%20infected%207h%20pi%20DAPI%202AmGL%20WGA_60xoilNA15_05_20SoRareconstruct32.2_20MLE%201.avi?csf=1&web=1&e=fM95t9

Movie S2: 3D reconstruction of 3A-expressing cells

https://solisservices-my.sharepoint.com/:v:/r/personal/a_schlemmer_students_uu_nl/Documents/_AS_instruction_006OSR_20MLE_movie.avi?csf=1&web=1&e=KfZ782

References

1. Baggen J, Thibaut HJ, Strating JRPM, van Kuppeveld FJM. The life cycle of non-polio enteroviruses and how to target it. Nat Rev Microbiol. 2018 Jun 6;16(6):368–81.

2. Nagy PD, Pogany J. The dependence of viral RNA replication on co-opted host factors. Nat Rev Microbiol. 2012 Feb 19;10(2):137–49.

3. Belov GA, van Kuppeveld FJ. (+)RNA viruses rewire cellular pathways to build replication organelles. Curr Opin Virol. 2012 Dec;2(6):740–7.

4. Miller S, Krijnse-Locker J. Modification of intracellular membrane structures for virus replication. Nat Rev Microbiol [Internet]. 2008 May;6(5):363–74. Available from: http://www.nature.com/articles/nrmicro1890

5. Belov GA, Nair V, Hansen BT, Hoyt FH, Fischer ER, Ehrenfeld E. Complex Dynamic Development of Poliovirus Membranous Replication Complexes. J Virol. 2012 Jan;86(1):302–12.

6. Limpens RWAL, van der Schaar HM, Kumar D, Koster AJ, Snijder EJ, van Kuppeveld FJM, et al. The Transformation of Enterovirus Replication Structures: a Three-Dimensional Study of Single- and Double-Membrane Compartments. mBio. 2011 Nov;2(5).

7. Ilnytska O, Santiana M, Hsu NY, Du WL, Chen YH, Viktorova EG, et al. Enteroviruses Harness the Cellular Endocytic Machinery to Remodel the Host Cell Cholesterol Landscape for Effective Viral Replication. Cell Host Microbe. 2013 Sep;14(3):281–93.

8. Strating JR, van Kuppeveld FJ. Viral rewiring of cellular lipid metabolism to create membranous replication compartments. Curr Opin Cell Biol. 2017 Aug;47:24–33.

9. Wessels E, Duijsings D, Notebaart RA, Melchers WJG, van Kuppeveld FJM. A Proline-Rich Region in the Coxsackievirus 3A Protein Is Required for the Protein To Inhibit Endoplasmic Reticulum-to-Golgi Transport. J Virol. 2005 Apr 15;79(8):5163–73.

10. Greninger AL, Knudsen GM, Betegon M, Burlingame AL, DeRisi JL. The 3A Protein from Multiple Picornaviruses Utilizes the Golgi Adaptor Protein ACBD3 To Recruit PI4KIIIβ. J Virol. 2012 Apr;86(7):3605–16.

11. Lyoo H, van der Schaar HM, Dorobantu CM, Rabouw HH, Strating JRPM, van Kuppeveld FJM. ACBD3 is an essential pan-enterovirus host factor that mediates the interaction between viral 3A protein and cellular protein PI4KB. mBio. 2019 Jan 1;10(1).

12. Horova V, Lyoo H, Różycki B, Chalupska D, Smola M, Humpolickova J, et al. Convergent evolution in the mechanisms of ACBD3 recruitment to picornavirus replication sites. PLoS Pathog. 2019 Aug 5;15(8):e1007962.

13. Klima M, Tóth DJ, Hexnerova R, Baumlova A, Chalupska D, Tykvart J, et al. Structural insights and in vitro reconstitution of membrane targeting and activation of human PI4KB by the ACBD3 protein. Sci Rep. 2016 Jul 24;6(1):23641.

14. Balla A, Tuymetova G, Tsiomenko A, Várnai P, Balla T. A Plasma Membrane Pool of Phosphatidylinositol 4-Phosphate Is Generated by Phosphatidylinositol 4-Kinase Type-III Alpha: Studies with the PH Domains of the Oxysterol Binding Protein and FAPP1. Mol Biol Cell. 2005 Mar;16(3):1282–95.

15. van der Schaar HM, Dorobantu CM, Albulescu L, Strating JRPM, van Kuppeveld FJM. Fat(al) attraction: Picornaviruses Usurp Lipid Transfer at Membrane Contact Sites to Create Replication Organelles. Vol. 24, Trends in Microbiology. Elsevier Ltd; 2016. p. 535–46.

16. Hsu NY, Ilnytska O, Belov G, Santiana M, Chen YH, Takvorian PM, et al. Viral Reorganization of the Secretory Pathway Generates Distinct Organelles for RNA Replication. Cell. 2010 May;141(5):799–811.

17. Roulin PS, Lötzerich M, Torta F, Tanner LB, van Kuppeveld FJM, Wenk MR, et al. Rhinovirus Uses a Phosphatidylinositol 4-Phosphate/Cholesterol Counter-Current for the Formation of Replication Compartments at the ER-Golgi Interface. Cell Host Microbe. 2014 Nov;16(5):677–90.

18. Mesmin B, Bigay J, Moser von Filseck J, Lacas-Gervais S, Drin G, Antonny B. A Four-Step Cycle Driven by PI(4)P Hydrolysis Directs Sterol/PI(4)P Exchange by the ER-Golgi Tether OSBP. Cell. 2013 Nov;155(4):830–43.

19. Albulescu L, Wubbolts R, Kuppeveld FJM, Strating JRPM. Cholesterol shuttling is important for RNA replication of coxsackievirus B3 and encephalomyocarditis virus. Cell Microbiol. 2015 Aug 10;17(8):1144–56.

20. Yang X, Cheng A, Wang M, Jia R, Sun K, Pan K, et al. Structures and Corresponding Functions of Five Types of Picornaviral 2A Proteins. Front Microbiol. 2017 Jul 21;8.

21. Serganov AA, Udi Y, Stein ME, Patel V, Fridy PC, Rice CM, et al. Proteomic elucidation of the targets and primary functions of the picornavirus 2A protease. Journal of Biological Chemistry. 2022 Jun;298(6):101882.

22. Wang L, Xie W, Zhang L, Li D, Yu H, Xiong J, et al. CVB3 Nonstructural 2A Protein Modulates SREBP1a Signaling via the MEK/ERK Pathway. J Virol. 2018 Dec 15;92(24).

23. Nchoutmboube JA, Viktorova EG, Scott AJ, Ford LA, Pei Z, Watkins PA, et al. Increased Long Chain acyl-Coa Synthetase Activity and Fatty Acid Import Is Linked to Membrane Synthesis for Development of Picornavirus Replication Organelles. PLoS Pathog. 2013 Jun 6;9(6):e1003401.

24. Viktorova EG, Nchoutmboube JA, Ford-Siltz LA, Iverson E, Belov GA. Phospholipid synthesis fueled by lipid droplets drives the structural development of poliovirus replication organelles. PLoS Pathog. 2018 Aug 27;14(8):e1007280.

25. Melia CE, Peddie CJ, de Jong AWM, Snijder EJ, Collinson LM, Koster AJ, et al. Origins of Enterovirus Replication Organelles Established by Whole-Cell Electron Microscopy. mBio. 2019 Jun 25;10(3).

26. Gao R, Asano SM, Boyden ES. Q&A: Expansion microscopy. BMC Biol. 2017 Dec 19;15(1):50.

27. Wassie AT, Zhao Y, Boyden ES. Expansion microscopy: principles and uses in biological research. Vol. 16, Nature Methods. Nature Publishing Group; 2019. p. 33–41.

28. Damstra HG, Mohar B, Eddison M, Akhmanova A, Kapitein LC. Visualizing cellular and tissue ultrastructure using Ten-fold Robust Expansion Microscopy (TREx). Available from: https://doi.org/10.1101/2021.02.03.428837

29. Nijenhuis W, Damstra HGJ, van Grinsven EJ, Iwanski MK, Praest P, Soltani ZE, et al. Optical nanoscopy reveals SARS-CoV-2-induced remodeling of human airway cells. Available from: https://doi.org/10.1101/2021.08.05.455126

30. Azuma T, Kei T. Super-resolution spinning-disk confocal microscopy using optical photon reassignment. Opt Express. 2015 Jun 1;23(11):15003.

31. Diel EE, Lichtman JW, Richardson DS. Publisher Correction: Tutorial: avoiding and correcting sample-induced spherical aberration artifacts in 3D fluorescence microscopy. Nat Protoc. 2021 Jul 2;16(7):3736–3736.

32. Shinjuku Monolith NSS ku. Super Resolution for All Types of Live Cell Imaging. Tokyo: EvidentOlympus;

33. Jurriens D, van Batenburg V, Katrukha EA, Kapitein LC. Mapping the neuronal cytoskeleton using expansion microscopy. In: Methods in Cell Biology. Academic Press Inc.; 2021. p. 105–24.

34. Katrukha EA, Jurriens D, Salas Pastene DM, Kapitein LC. Quantitative mapping of dense microtubule arrays in mammalian neurons. Elife. 2021 Jul 27;10.

35. Mascheroni L, Scherer KM, Manton JD, Ward E, Dibben O, Kaminski CF. Combining sample expansion and light sheet microscopy for the volumetric imaging of virus-infected cells with super-resolution. Biomed Opt Express. 2020 Sep 1;11(9):5032.

36. Drelich L, Aboulouard S, Franck J, Salzet M, Fournier I, Wisztorski M. Toward High Spatially Resolved Proteomics Using Expansion Microscopy. Anal Chem. 2021 Sep 14;93(36):12195–203.

37. Raquel L. Doval, Heyrhyoung Lyoo, Frank Kuppeveld. Visualizing the recruitment of host factors to enterovirus replication organelles with advanced immunofluorescence microscopy. Utrecht; 2021.

38. Ons M'Saad, Ravikiran Kasula, Ilona Kondratiuk, Phylicia Kidd, Hanieh Falahati, Juliana E. Gentile, et al. All-optical visualization of specific molecules in the ultrastructural context of brain tissue. BioRxiv. 2022 Apr 5;

39. Ons M'Saad, Ravikiran Kasula, Ilona Kondratiuk, Phylicia Kidd, Hanieh Falahati, Juliana E. Gentile, et al. All-optical visualization of specific molecules in the ultrastructural context of brain tissue. BioRxiv. 2022;

40. Campbell BC, Nabel EM, Murdock MH, Lao-Peregrin C, Tsoulfas P, Blackmore MG, et al. mGreenLantern: a bright monomeric fluorescent protein with rapid expression and cell filling properties for neuronal imaging. Proceedings of the National Academy of Sciences. 2020 Dec 18;117(48):30710–21.

41. Melia CE, van der Schaar HM, Lyoo H, Limpens RWAL, Feng Q, Wahedi M, et al. Escaping Host Factor PI4KB Inhibition: Enterovirus Genomic RNA Replication in the Absence of Replication Organelles. Cell Rep. 2017 Oct;21(3):587–99.

42. Jackson T, Belsham GJ. Review picornaviruses: A view from 3a. Vol. 13, Viruses. MDPI AG; 2021.

43. Towner JS, Ho T v., Semler BL. Determinants of Membrane Association for Poliovirus Protein 3AB. Journal of Biological Chemistry. 1996 Oct;271(43):26810–8.

44. Fujita K, Krishnakumar SS, Franco D, Paul A v., London E, Wimmer E. Membrane Topography of the Hydrophobic Anchor Sequence of Poliovirus 3A and 3AB Proteins and the Functional Effect of 3A/3AB Membrane Association upon RNA Replication. Biochemistry. 2007 May 1;46(17):5185–99.

45. Wessels E, Duijsings D, Lanke KHW, van Dooren SHJ, Jackson CL, Melchers WJG, et al. Effects of Picornavirus 3A Proteins on Protein Transport and GBF1-Dependent COP-I Recruitment. J Virol. 2006 Dec;80(23):11852–60.

46. Jago CB, Yates J, Olsen Saraiva Camara N, Lechler RI, Lombardi G. Differential expression of CTLA-4 among T cell subsets. Clin Exp Immunol. 2004 May 4;136(3):463–71.

47. Albrecht Thomas, Fons Michael, Boldogh Istvan, Rabson Alan. Effects on Cells [Internet]. 4th ed. Baron S, editor. Vol. 4th edition, Medical Microbiology. Galveston (TX): University of Texas Medical Branch at Galveston; 1996 [cited 2022 Aug 16]. Available from: https://www.ncbi.nlm.nih.gov/books/NBK7979/

48. Aho, Mäntylä, Ekman, Hakanen, Mattola, Chen, et al. Quantitative Microscopy Reveals Stepwise Alteration of Chromatin Structure during Herpesvirus Infection. Viruses. 2019 Oct 11;11(10):935.

49. Gao R, Yu CC, Gao L, Piatkevich KD, Neve RL, Munro JB, et al. A highly homogeneous polymer composed of tetrahedron-like monomers for high-isotropy expansion microscopy. Nat Nanotechnol. 2021 Jun 29;16(6):698–707.

50. Laporte MH, Klena N, Hamel V, Guichard P. Visualizing the native cellular organization by coupling cryofixation with expansion microscopy (Cryo-ExM). Nat Methods. 2022 Feb 13;19(2):216–22.

51. Yu S, Xiong G, Zhao S, Tang Y, Tang H, Wang K, et al. Nanobodies targeting immune checkpoint molecules for tumor immunotherapy and immunoimaging (Review). Int J Mol Med. 2020 Dec 14;47(2):444–54.

52. Tinnefeld P, Cordes T. "Self-healing" dyes: intramolecular stabilization of organic fluorophores. Nat Methods. 2012 May 27;9(5):426–7.

53. Wessels E, Duijsings D, Niu TK, Neumann S, Oorschot VM, de Lange F, et al. A Viral Protein that Blocks Arf1-Mediated COP-I Assembly by Inhibiting the Guanine Nucleotide Exchange Factor GBF1. Dev Cell. 2006 Aug;11(2):191–201.

54. Schindelin J, Arganda-Carreras I, Frise E, Kaynig V, Longair M, Pietzsch T, et al. Fiji: an open-source platform for biological-image analysis. Nat Methods. 2012 Jul 28;9(7):676–82.